Dirty MIMO Transmitters: Does It Matter?

Peter Händel, *Senior Member, IEEE*, and Daniel Rönnow, *Member, IEEE*

***Abstract*— The radio frequency transmitter is a key component in contemporary multiple-input multiple-output (MIMO) orthogonal frequency-division multiplexing systems. A detailed study of a 2×2 MIMO transmitter subjected to correlated input data streams, nonlinear distortion, thermal noise, and crosstalk is provided by stochastic modeling. The effects of correlated input streams, crosstalk, and nonlinearities are studied in detail and exemplified both by approximate expressions and numerical simulations. Key results include exact and approximate expressions for the normalized mean-squared error (NMSE) for systems with or without digital predistortion; the relationship between NMSE and the signal-to-noise-and-distortion ratio, the properties of the distortion noise, and a novel design for power amplifier back-off for MIMO transmitters subject to crosstalk. The theoretical derivations are illustrated by numerical examples and simulation results, and their relationships to the state-of-the-art research are discussed.**

***Index Terms*— Orthogonal frequency division multiplexing (OFDM), input back-off, power amplifier, optimization, Bussgang theory.**

I. Introduction

STOCHASTIC baseband modeling is a powerful tool for modeling the behavior and performance of a radio frequency transmitter subject to impairments or so called dirty radio effects [1]. Early work describing single-input-single-output (SISO) transmitters include [2] and [3], where different soft and hard nonlinearities subject to Gaussian excitation are considered. More recent work on SISO systems, which explicitly consider orthogonal frequency domain multiplexing (OFDM), include e.g. [4] which discusses the spectral characteristics of the transmitted signal, and [5] considering optimal power amplifier back-off.

Early work on multiple-input-multiple-output (MIMO) systems includes [6], where uncorrelated input streams and decoupled transmitter chains were considered. The case of correlated input streams was considered in [7], where the correlation of the distortion noise of a crosstalk-free 2×2 MIMO radio frequency system was considered, both theoretically and experimentally. It was shown that for correlated input streams, the phase of the correlation coefficient is preserved for the distortion noise, but that the magnitude decays. The theoretical predictions on the spatial direction of the distortion noise were complemented by radio frequency test-bed measurements based on the set-up in [8]. A favorable agreement between theoretical predictions and measurement results was presented in [7], and provided support for the applicability of the theoretical framework. For MIMO systems analysis, the work [7] has gained recognition to support simplified transmission models, e.g. as presented in the text book [9]. The work [7] has recently also gained the attention of the massive MIMO community. For example, in the seminal work [10], the authors assume that the distortion noise and useful signal have different spatial signatures, based on the observation in [7] that the magnitude of the correlation coefficient decays by the power of three. Accordingly, this assumption is now well established in the research community, e.g. referred to in the massive MIMO survey [11], and text book [12]. However, the assumption that hardware impairments and transmitted streams are uncorrelated is also questioned, by independent research groups, e.g. in [13] and [14], and thus a deeper understanding of the behavior of dirty MIMO transmitters is required.

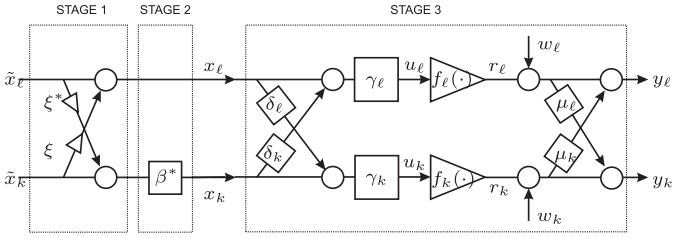

Fig. 1. The baseband model describing possible correlated input OFDM modulated streams exciting a dirty 2×2 MIMO transmitter.

In the current work, a deeper understanding of the behavior of dirty MIMO transmitters (see, Fig. 1) is envisaged, motivated by trends such as allocating the radio frequency branches on the same chip [15], and MIMO crosstalk modeling, calibration, and cancelation [16]–[19]. Employing a classical and powerful approach within a stochastic and static framework, a 2×2 OFDM-modulated MIMO transmitter is considered and studied in detail, and is subjected to correlated input streams, crosstalk, and nonlinear compression. The analysis complements previous analyses such as [20] and [21] which use a stochastic framework and take the temporal dimension into account. The employed approach provides insights into the problem at hand in a compact way. In addition, it complements the work on characterization and

Manuscript received January 10, 2018; revised March 29, 2018 and May 30, 2018; accepted May 31, 2018. Date of publication June 12, 2018; date of current version August 10, 2018. The associate editor coordinating the review of this paper and approving it for publication was A. Bletsas. *(Corresponding author: Peter Händel.)*

P. Händel is with the Department of Information Science and Engineering, KTH Royal Institute of Technology, 10044 Stockholm, Sweden (e-mail: ph@kth.se).

D. Rönnow is with the Department of Electronics, Mathematics and Natural Sciences, University of Gävle, 80176 Gävle, Sweden (e-mail: daniel.ronnow@hig.se).

Color versions of one or more of the figures in this paper are available online at http://ieeexplore.ieee.org.

Digital Object Identifier 10.1109/TWC.2018.2843764

the modeling of hardware impairments in MIMO transmitters that use tailored signals, dedicated measurement set-ups, and elaborate identification techniques, such as the measurement of the Volterra kernels [22] or behaviorial modeling based on measured input/output signals [16].

The paper is motivated by the plurality of results and insights that are derived for the considered nonlinear MIMO transmitter model subjected to crosstalk and correlated input streams. In short, by the adopted methodology, it is shown that:

- *Transmitter performance:* Crosstalk degrades the performance of a 2×2 MIMO transmitter. This claim is quantified by describing the 2×2 MIMO transmitter as two decoupled SISO transmitters with degraded signal-to-noise-ratio. This observation relates to the question given in the title of this paper, i.e. if the performance of an 'equivalent system' with two decoupled (no crosstalk) SISO transmitters is fulfilling our requirements, then the 'dirty MIMO-effect' does not matter. More details on this subject are provided at the end of the paper.
- *Transmitter operation:* SISO-based methodologies for power amplifier back-off determination are valid for a 2×2 MIMO transmitter subject to crosstalk. However, schemes taking the crosstalk into account may be favorable, because they typically allow for the operation of the transmitter with increased energy efficiency.
- *Effects by data streams: On average*, the transmitter performance is degraded equally by crosstalk for both correlated and uncorrelated data streams. Because of the crosstalk, data streams with a specific correlation between the two channels may degrade or improve the performance of the transmitter.
- *Effects on spatial direction:* Thermal noise decorrelates the spatial direction of the distortions relative to the desired signal. Crosstalk steers the spatial direction of the data streams and nonlinear distortion induced by the power amplifiers somewhat towards zero degrees. Accordingly, the work provides additional support to the simplified transmission model that have been popularized in work such as [9], [11], and [12].

The above results are discussed in detail in the paper, which is organized as follows. In Sec. II, the stochastic model in Fig. 1, which describes a dirty 2×2 MIMO transmitter for OFDM transmission, is introduced. Sec. III presents the considered figures of merit and their general properties. In Sec. IV, a third order polynomial nonlinear system is studied in detail. In Sec. V, performance optimization by input power back-off and the effects of digital predistortion (DPD) are considered. Numerical examples which provide additional insights are considered in Sec. VI. Conclusions are drawn in Sec.VII.

II. System Model

The model set-up is shown in Fig. 1. It is divided into three stages. The model contains the main hardware impairments in a MIMO transmitter [23], but imperfections in the signal generation are not included. The first stage models the OFDM modulated communication streams, which are possibly correlated. Accordingly, the first stage is built up by the zero mean complex Gaussian uncorrelated sources $\{\tilde{x}_\ell, \tilde{x}_k\}$, mixed via the correlation coefficient ξ. Details concerning the modeling of OFDM signals as Gaussian sources can be found in [24]. The second stage, displayed in Fig. 1, includes a scalar attenuation β^* on the k:th channel, where * denotes the complex conjugate. The second stage is introduced to handle, e.g. beamforming, or a laboratory use case where only one of the channels is excited. In addition, the second stage can be replaced by a module for DPD, to combat the crosstalk and nonlinear distortion of the third stage. DPD will briefly be discussed in this paper. The third stage describes a 2×2 transmitter, which is subject to both input and output crosstalk, gain variations, nonlinear distortion, and thermal noise, and is explained in detail in the following sections.

A. Signal Model

By Fig. 1, the ℓ:th transmitter output is given by

$$y_\ell = r_\ell + w_\ell + \mu_k\,(r_k + w_k), \tag{1}$$

where r_ℓ is the in-channel amplifier output, r_k is the adjacent channel amplifier output that is leaking into the channel, and $\{w_\ell, w_k\}$ are the thermal noises. It should be noted that the model (1) is static, and thus the time index is not explicitly shown.

To a large extent, the model in Fig. 1 is symmetrical with respect to ℓ and k, that is $k = 1 + \mathrm{mod}_2(\ell)$, or $k = 2$ for $\ell = 1$, and *vice versa*. Accordingly, only the equations for the ℓ:th channel are presented. For the few asymmetries in the model, the corresponding equations are explicitly given and separate equations are presented for the ℓ:th and k:th channel. The scalars $\{\mu_\ell, \mu_k\} \in \mathbb{C}$ are the parameters which determine the output crosstalk. The thermal noise sources w_ℓ and w_k are assumed to be jointly independent zero-mean Gaussian with a common variance σ_w^2.

The model of the power amplifier in each branch is divided into a gain γ_ℓ and a static nonlinearity $f_\ell(\cdot)$, that is

$$r_\ell = f_\ell(u_\ell), \tag{2}$$

where $f_\ell(\cdot)$ is the characteristic function of a static nonlinearity, with a 0 dB small signal gain or $f_\ell(u)/u \to 1$ as $|u| \to 0$, with $u \in \mathbb{C}$. Furthermore,

$$u_\ell = \gamma_\ell\, p_\ell. \tag{3}$$

In the current discussion, no specific form of $f_\ell(\cdot)$ in (2) is yet considered, besides its unity small signal gain. Further, u_ℓ is the baseband excitation to the nonlinearity $f_\ell(\cdot)$. The gain γ_ℓ is excited by a signal which is affected by an input cross talk, that is

$$p_\ell = x_\ell + \delta_k\, x_k, \tag{4}$$

where $\{\delta_\ell, \delta_k\} \in \mathbb{C}$ are the parameters of the input crosstalk. The crosstalk is typically caused by coupling between the transmission lines on the circuit board. Hence, it is modeled by a linear reciprocal network (see, e.g. [25]), i.e. $\delta_\ell = \delta_k$ and $\mu_\ell = \mu_k$. The channel indices k, ℓ are kept, to make the interpretation of the result easier. Energy conservation gives that $|\delta_\ell| < 1$ and $|\mu_\ell| < 1$. Notice that the gains γ_ℓ and

γ_k contain not only the gain of the amplifiers, but also the attenuation of x_ℓ and x_k due to crosstalk and losses. The latter effects are in most cases negligible, and not explicitly modeled. The noise of the amplifier is modeled as it was added after the nonlinearity [25].

The inputs $\{x_\ell,\, x_k\}$ model the possible correlated OFDM modulated streams. Since the power levels of $\{x_\ell,\, x_k\}$ determine the power amplifier back-offs, their average power is set as reference, that is $\mathbb{E}[x_\ell\, x_\ell^*] = \sigma_x^2$ and $\mathbb{E}[x_k\, x_k^*] = |\beta|^2\, \sigma_x^2$, which are fixed independently of the actual correlation ξ. Here, $\mathbb{E}[\cdot]$ denotes statistical expectation.

Finally, with reference to Fig. 1, the correlation of the transmitted OFDM streams is described by

$$x_\ell = \tilde{x}_\ell + \xi\, \tilde{x}_k, \tag{5}$$

$$x_k = \beta^*(\tilde{x}_k + \xi^*\, \tilde{x}_\ell). \tag{6}$$

With $\{x_\ell\}$ and its average power σ_x^2 set as reference, it is a straightforward exercise (see, Appendix A) to show that the covariance $\mathbb{E}[x_\ell\, x_k^*]$ reads $\mathbb{E}[x_\ell\, x_k^*] = 2\,\xi\,\beta\,\sigma_x^2/(1+|\xi|^2)$.

B. Resolving the Nonlinearity $f_\ell(\cdot)$

In order to perform the analysis, the expression of the amplifier output r_ℓ in (2) is the sum of an attenuated replica s_ℓ of the input u_ℓ, and of the zero mean distortion noise v_ℓ, where v_ℓ and s_ℓ are jointly uncorrelated. Thus,

$$r_\ell = s_\ell + v_\ell, \tag{7}$$

where,

$$s_\ell = \alpha_\ell\, u_\ell. \tag{8}$$

In (8), $\alpha_\ell \in \mathbb{C}$ is an attenuation to be determined by the Bussgang theory [26]. Starting with (7) and (8) and considering the covariance $\mathbb{E}[r_\ell\, u_\ell^*]$, then

$$\mathbb{E}[r_\ell\, u_\ell^*] = \alpha_\ell\, \mathbb{E}[u_\ell\, u_\ell^*] + \mathbb{E}[v_\ell\, u_\ell^*]. \tag{9}$$

For the distortion noise v_ℓ to be uncorrelated with the amplifier input u_ℓ, it is, by construction, required that the second term in (9) equals zero, that is $\mathbb{E}[v_\ell\, u_\ell^*] \equiv 0$. Reordering the terms in (9) provides the Bussgang attenuation

$$\alpha_\ell = \frac{\mathbb{E}[r_\ell\, u_\ell^*]}{\mathbb{E}[u_\ell\, u_\ell^*]}. \tag{10}$$

In other words, the particular choice of α_ℓ in (10) divides the output $r_\ell = f_\ell(u_\ell)$ into a sum of an attenuated version of the input stream and an uncorrelated distortion noise [26].

Inserting the linearized description (7)-(8) of r_ℓ into (1), using (3)-(4), a straightforward calculation yields

$$y_\ell = \underbrace{(\alpha_\ell\,\gamma_\ell + \alpha_k\,\gamma_k\,\mu_k\,\delta_\ell)\, x_\ell}_{\text{attenuated source}} + \underbrace{(\alpha_\ell\,\gamma_\ell\,\delta_k + \alpha_k\,\gamma_k\,\mu_k)\, x_k}_{\text{channel leakage}} + \underbrace{v_\ell + \mu_k\, v_k}_{\text{distortion: } d_\ell} + \underbrace{w_\ell + \mu_k\, w_k}_{\text{thermal noise: } n_\ell}. \tag{11}$$

In order to make the notation more compact, the augmented distortion noise $d_\ell = v_\ell + \mu_k\, v_k$, and the augmented thermal noise $n_\ell = w_\ell + \mu_k\, w_k$ were introduced in (11).

Finally, by defining the error signal as e_ℓ as $e_\ell = y_\ell - \gamma_\ell\, x_\ell$, then resolving the input streams $\{x_\ell,\, x_k\}$ into the uncorrelated $\{\tilde{x}_\ell,\, \tilde{x}_k\}$ via (5)-(6), the error e_ℓ reads

$$e_\ell = \theta_\ell\, \tilde{x}_\ell + \theta_k\, \tilde{x}_k + d_\ell + n_\ell, \tag{12}$$

where

$$\theta_\ell = \gamma_\ell(\alpha_\ell - 1) + \alpha_k\,\gamma_k\,\mu_k\,\delta_\ell + (\alpha_\ell\,\gamma_\ell\,\delta_k + \alpha_k\,\gamma_k\,\mu_k)\beta^*\xi^*, \tag{13}$$

$$\theta_k = (\gamma_\ell(\alpha_\ell - 1) + \alpha_k\,\gamma_k\,\mu_k\,\delta_\ell)\xi + (\alpha_\ell\,\gamma_\ell\,\delta_k + \alpha_k\,\gamma_k\,\mu_k)\beta^*. \tag{14}$$

The θ's are functions of the gains, crosstalk, input correlation, and system nonlinearities.

III. Figures of Merit

The normalized mean squared error (NMSE) is taken as a primary figure of merit to measure the performance, by describing the quality of the service of the transmitted streams at the level of the transmitter. In addition, the properties of the cross-channel distortion noise are studied via the normalized error covariance (NEC).

A. NMSE

The NMSE is defined by

$$\text{NMSE}_\ell \stackrel{\triangle}{=} \frac{\mathbb{E}[e_\ell\, e_\ell^*]}{|\gamma_\ell|^2\, \sigma_x^2}. \tag{15}$$

In (15), the error e_ℓ in (12) consists of four jointly uncorrelated terms. Accordingly, the NMSE (15) follows directly:

$$\text{NMSE}_\ell = \frac{|\theta_\ell|^2 + |\theta_k|^2}{|\gamma_\ell|^2\,(1+|\xi|^2)} + \frac{\mathbb{E}[d_\ell\, d_\ell^*]}{|\gamma_\ell|^2\,\sigma_x^2} + \frac{(1+|\mu_k|^2)\,\sigma_w^2}{|\gamma_\ell|^2\,\sigma_x^2}, \tag{16}$$

where the first term utilizes that $\mathbb{E}[\tilde{x}_\ell\, \tilde{x}_\ell^*] = \mathbb{E}[\tilde{x}_k\, \tilde{x}_k^*] = \sigma_x^2/(1+|\xi|^2)$ (see Appendix A), and the third the definition of the augmented noise (11). The second term $\mathbb{E}[d_\ell\, d_\ell^*]$ in (16) is the variance of the augmented distortion noise in (11), which is expressed in terms of the distortion noise as

$$\mathbb{E}[d_\ell\, d_\ell^*] = \mathbb{E}[v_\ell\, v_\ell^*] + 2\Re[\,\mu_k^*\, \mathbb{E}[v_\ell\, v_k^*]\,] + |\mu_k|^2\, \mathbb{E}[v_k\, v_k^*], \tag{17}$$

where $z + z^* = 2\Re[z]$ for $z \in \mathbb{C}$, and $\Re[z]$ denotes the real part of the complex-valued z. The results (16)-(17) are generic. For specific results, the nonlinearities have to be modeled and specified. However, some generic expressions can be obtained under a weak nonlinearity assumption and a small amount of crosstalk, as discussed below.

B. NMSE for Almost Ideal Systems

Consider a 2×2 transmitter where the crosstalk is assumed to be small and the nonlinearities vague. In other words, $f_\ell(\cdot)$ is close to linear, and the crosstalk parameters $\{\delta_\ell,\ \delta_k\}$ and $\{\mu_\ell,\ \mu_k\}$ are close to zero. An approximate expression for the NMSE can then be obtained. For $f_\ell(z) \approx z$, the Bussgang attenuation is close to unity or $\alpha_\ell \simeq 1 + \Delta_\ell$, where $\simeq$ denotes

an equality where only the dominant terms have been retained. To further simplify the analysis, two scenarios are studied, namely *(i)* uncorrelated input streams, that is $\xi = 0$, and *(ii)* a unity-magnitude correlation coefficient, that is $\xi = e^{i\phi}$.

First, let $\xi = 0$, then the NMSE in (16) reduces to

$$\text{NMSE}_\ell \simeq |\Delta_\ell|^2 + |\beta|^2\,|\delta_k + \mu_k|^2 + \frac{\mathbb{E}[v_\ell\, v_\ell^*]}{|\gamma|^2\,\sigma_x^2} + \frac{\sigma_w^2}{|\gamma|^2\,\sigma_x^2}, \tag{18}$$

where θ_ℓ and θ_k in (13)-(14) reduce to $\theta_\ell \simeq \gamma\,\Delta_\ell$, and $\theta_k \simeq \gamma(\delta_k + \mu_k)\beta^*$, and γ denotes the nominal gain. The approximation $\mathbb{E}[d_\ell\, d_\ell^*] \simeq \mathbb{E}[v_\ell\, v_\ell^*]$ follows from (17).

Now, consider $\xi = e^{i\phi}$, that is $|\xi| = 1$. Then, the NMSE in (16) reduces to

$$\text{NMSE}_\ell \simeq |\Delta_\ell + (\delta_k + \mu_k)\beta^*\, e^{-i\phi}|^2 + \frac{\mathbb{E}[v_\ell\, v_\ell^*]}{|\gamma|^2\,\sigma_x^2} + \frac{\sigma_w^2}{|\gamma|^2\,\sigma_x^2}. \tag{19}$$

Comparing (19) with (18) reveals

$$\text{NMSE}_\ell|_{|\xi|=1} = \text{NMSE}_\ell|_{\xi=0} + T, \tag{20}$$

where $\text{NMSE}_\ell|_{\xi=0}$ is given by (18), and the term T reads

$$T = 2\Re[\Delta_\ell^*\,(\delta_k + \mu_k)\beta^*\, e^{-i\phi}]. \tag{21}$$

Accordingly, the phase of the correlation coefficient influences the NMSE. Assuming all phases ϕ are equally probable, that is $\xi = e^{i\Phi}$ where Φ is a uniformly distributed stochastic variable in $[-\pi, \pi]$, which is independent of all other stochastic quantities. Then, the expected value $\mathbb{E}[T] = 0$. *Accordingly, on average, the phase of the correlation coefficient does not influence the NMSE. However, for particular correlation angles ϕ, the term T may take both positive and negative values.*

C. Normalized Error Covariance

The cross-channel properties of the distortion noise are measured by the NEC

$$\text{NEC}_\ell \triangleq \frac{\mathbb{E}[e_\ell\, e_k^*]}{|\gamma_\ell|\,|\gamma_k|\,\sigma_x^2}. \tag{22}$$

Here, e_k reads $e_k = \vartheta_\ell\,\tilde{x}_\ell + \vartheta_k\,\tilde{x}_k + d_k + n_k$, where

$$\vartheta_\ell = (\gamma_k(\alpha_k - 1) + \alpha_\ell\,\gamma_\ell\,\mu_\ell\,\delta_k)\beta^*\,\xi^* + \alpha_k\,\gamma_k\,\delta_\ell + \alpha_\ell\,\gamma_\ell\,\mu_\ell, \tag{23}$$

$$\vartheta_k = (\gamma_k(\alpha_k - 1) + \alpha_\ell\,\gamma_\ell\,\mu_\ell\,\delta_k)\beta^* + (\alpha_k\,\gamma_k\,\delta_\ell + \alpha_\ell\,\gamma_\ell\,\mu_\ell)\xi. \tag{24}$$

Accordingly, the NEC (22) reads

$$\text{NEC}_\ell = \frac{\theta_\ell\,\vartheta_\ell^* + \theta_k\,\vartheta_k^*}{|\gamma_\ell|\,|\gamma_k|\,(1 + |\xi|^2)} + \frac{\mathbb{E}[d_\ell\, d_k^*]}{|\gamma_\ell|\,|\gamma_k|\,\sigma_x^2} + \frac{(\mu_\ell^* + \mu_k)\,\sigma_w^2}{|\gamma_\ell|\,|\gamma_k|\,\sigma_x^2}. \tag{25}$$

For an almost ideal MIMO system, the $\{\delta_\ell,\, \delta_k\}$, $\{\mu_\ell,\, \mu_k\}$ are all close to zero, and $\{\alpha_\ell,\, \alpha_k\}$ are both close to unity. Thus, the numerator of the first term in (25), which consists of second order or higher products, is negligible in comparison with the other two. The numerator of the second term in (25) follows from (11), that is

$$\mathbb{E}[d_\ell\, d_k^*] = \mathbb{E}[v_\ell\, v_k^*] + \mu_\ell^*\,\mathbb{E}[v_\ell\, v_\ell^*] + \mu_k\,\mathbb{E}[v_k\, v_k^*] + \mu_k\mu_\ell^*\,\mathbb{E}[v_\ell\, v_k^*]^*. \tag{26}$$

With (26) and neglecting all higher order terms in (25), an approximate NEC expression for an almost ideal MIMO system is given by

$$\text{NEC}_\ell \simeq \frac{\mathbb{E}[v_\ell\, v_k^*]}{|\gamma|^2\,\sigma_x^2}. \tag{27}$$

D. A Remark on Methodology

Based on the presented framework, other figures of merit can also be analyzed, including measures based on the input-output covariance $\mathbb{E}[e_\ell\, x_\ell^*]$ and cross-covariance $\mathbb{E}[e_\ell\, x_k^*]$. However, such figures of merit are beyond the scope of the present paper.

The employed methodology is summarized as follows. For a given set of nonlinearities, the Bussgang attenuations $\{\alpha_\ell,\, \alpha_k\}$ were calculated. Based on these calulations, the properties of the distortion noises could be determined, that is $\mathbb{E}[v_\ell\, v_\ell^*]$, $\mathbb{E}[v_k\, v_k^*]$ and covariance $\mathbb{E}[v_\ell\, v_k^*]$. Finally, the properties of the augmented distortion noises were calculated, followed by calculations of the figures of merit such as the NMSE. The Bussgang attenuation and the properties of the distortion noise both depend on the properties of the inputs $\{u_\ell,\, u_k\}$ exciting the nonlinearities (see Fig. 1). Accordingly, an analysis based on the Bussgang theory relies on the properties of $\{u_\ell,\, u_k\}$, which are the variances $\mathbb{E}[u_\ell\, u_\ell^*]$ and $\mathbb{E}[u_k\, u_k^*]$, and the covariance $\mathbb{E}[u_\ell\, u_k^*]$. In turn, these properties are functions of the preceding linear network in Fig. 1. The corresponding derivations are provided in Appendix B.

IV. MIMO System Analysis

A third order static model captures the main nonlinear distortion of solid state amplifiers [27].

Consider a pair of third order nonlinearities $\{f_\ell(\cdot),\, f_k(\cdot)\}$ excited by the zero-mean complex-Gaussian inputs $\{u_\ell,\, u_k\}$, respectively. Further, consider a third order nonlinearity $f_\ell(\cdot)$ in (2) with unity small signal gain $f_\ell(z) = z + \rho_\ell\, z\,|z|^2$ for $z \in \mathbb{C}$, that is the power amplifier output obeys

$$r_\ell = u_\ell + \rho_\ell\, u_\ell\,|u_\ell|^2, \tag{28}$$

where ρ_ℓ (with $\rho_\ell \in \mathbb{C}$) is the amplifier's compression parameter. The model can be related to metrics as the third order intercept point and 1dB compression point [25].

A. 1dB Compression Point

Starting with (28), the output power reads

$$\mathbb{E}[r_\ell\, r_\ell^*] = \mathbb{E}[(u_\ell + \rho_\ell\, u_\ell\,|u_\ell|^2)(u_\ell^* + \rho_\ell^*\, u_\ell^*\,|u_\ell|^2)]. \tag{29}$$

To resolve the fourth order moment in (29), note that the moments of a complex-valued Gaussian variable u_ℓ obey $\mathbb{E}[(u_\ell\, u_\ell^*)^n] = n!\,\mathbb{E}[u_\ell\, u_\ell^*]^n$, for positive integers n,

where ! denotes the factorial operation [28]. Now, a straightforward calculation yields

$$\mathbb{E}[r_\ell\, r_\ell^*] = \mathbb{E}[u_\ell\, u_\ell^*] + 4\Re[\rho_\ell]\,\mathbb{E}[u_\ell\, u_\ell^*]^2 + 6|\rho_\ell|^2\,\mathbb{E}[u_\ell\, u_\ell^*]^3. \tag{30}$$

The 1dB compression point is defined by $\mathbb{E}[r_\ell\, r_\ell^*]/\mathbb{E}[u_\ell\, u_\ell^*] = 10^{-1/10}$, that is with $\sigma_u^2 = \mathbb{E}[u_\ell\, u_\ell^*]$ given by the solution to a second order equation, that is

$$\sigma_u^2 = -\frac{\Re[\rho_\ell]}{3|\rho_\ell|^2} \pm \frac{\sqrt{2\Re[\rho_\ell]^2 - 3|\rho_\ell|^2(1-10^{-1/10})}}{3\sqrt{2}\,|\rho_\ell|^2}. \tag{31}$$

For real-valued $\rho_\ell < 0$, (31) reduces to

$$\sigma_u^2 = \frac{1}{3|\rho_\ell|}\left(1 \pm \frac{\sqrt{-1+3\cdot 10^{-1/10}}}{\sqrt{2}}\right) = \frac{C_{\text{1dB}}}{|\rho_\ell|}, \tag{32}$$

where the constant $C_{\text{1dB}} \approx 0.056$. The solution corresponding to the minus sign is kept because the characteristic function $f_\ell(\cdot)$ is a concave function. Accordingly, employing the expression in (64) in Appendix B for $\sigma_u^2 = \mathbb{E}[u_\ell\, u_\ell^*]$, the 1dB compression point reads

$$\sigma_x^2 = \frac{1+|\xi|^2}{|1+\delta_k\,\beta^*\,\xi^*|^2 + |\xi+\delta_k\,\beta^*|^2}\,\frac{C_{\text{1dB}}}{|\rho_\ell|\,|\gamma_\ell|^2}. \tag{33}$$

One can note that significant crosstalk will influence the 1dB compression point negatively, and also that it depends on the input correlation ξ.

It is worth noting that the nonlinear compression is signal dependent, and thus the compression looks different depending on the characteristics of the input u_ℓ. The 1dB compression point in (33) differs from the traditional compression point defined and measured using sinewave test stimuli [25]. For OFDM streams modeled as complex Gaussian stochastic variables, the output power $\sigma_r^2 = \mathbb{E}[r_\ell\, r_\ell^*]$ (based on the third order model (28)) for real-valued $\rho_\ell < 0$ reads

$$\sigma_r^2 = \sigma_u^2 - 4|\rho_\ell|\,\sigma_u^4 + 6|\rho_\ell|^2\,\sigma_u^6, \tag{34}$$

where $\sigma_u^2 = \mathbb{E}[u_\ell\, u_\ell^*]$, and $\mathbb{E}[(u_\ell\, u_\ell^*)^n] = n!\,\sigma_u^{2n}$ were used. Now, consider a temporal narrow band signal $u_\ell(t) = \sigma_u\, e^{j\omega t}$, where ω denotes the angular frequency, t the time, and σ_u denotes the amplitude. At a given instant t, the narrow band signal equals a constant magnitude quantity. Thus, the output power σ_r^2 for (28) reads

$$\sigma_r^2 = \sigma_u^2 - 2|\rho_\ell|\,\sigma_u^4 + |\rho_\ell|^2\,\sigma_u^6. \tag{35}$$

The results (34)-(35) are visualized in Fig. 2 for a nonlinearity (28) with $\rho_\ell = -0.1$. From Fig. 2, one can note that when the amplifier enters compression, a higher compression is obtained for the OFDM-modulated signal compared with the narrow band tone.

B. Bussgang Attenuation α_ℓ

A direct calculation of the covariance between the output r_ℓ and the input u_ℓ in (28), yields

$$\begin{aligned}\mathbb{E}[r_\ell\, u_\ell^*] &= \mathbb{E}[u_\ell\, u_\ell^*] + \rho_\ell\,\mathbb{E}[(u_\ell\, u_\ell^*)^2] \\ &= \mathbb{E}[u_\ell\, u_\ell^*] + 2\,\rho_\ell\,\mathbb{E}[u_\ell\, u_\ell^*]^2.\end{aligned} \tag{36}$$

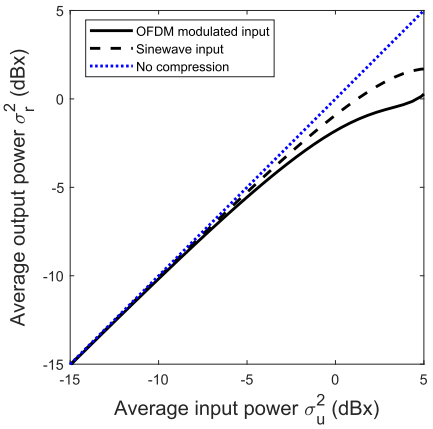

Fig. 2. Signal dependent compression for OFDM-modulated signal (solid black line) and single tone (dashed black line).

Accordingly, the Bussgang attenuation α_ℓ in (10) follows directly by dividing the covariance in (36) with $\mathbb{E}[u_\ell\, u_\ell^*]$, that is

$$\alpha_\ell = 1 + 2\rho_\ell\,\mathbb{E}[u_\ell\, u_\ell^*]. \tag{37}$$

In (37), the Bussgang gain $\alpha_\ell \in \mathbb{C}$, and the variance $\mathbb{E}[u_\ell\, u_\ell^*]$ is given by (64) in Appendix B.

C. Properties of the Distortion Noise

Now by (7)-(8), the distortion noise $v_\ell = r_\ell - \alpha_\ell\, u_\ell$ reads

$$v_\ell = \rho_\ell\, u_\ell\,(|u_\ell|^2 - 2\,\mathbb{E}[u_\ell\, u_\ell^*]), \tag{38}$$

where the right hand side follows from (28), (37), and a straightforward calculation. By construction, the distortion noise v_ℓ in (38) is uncorrelated with the input u_ℓ, but is clearly not stochastically independent.

With v_ℓ given by (38), $\mathbb{E}[v_\ell\, v_\ell^*]$, $\mathbb{E}[v_k\, v_k^*]$ and $\mathbb{E}[v_\ell\, v_k^*]$ are calculated as functions of the properties of the given excitations, that is $\mathbb{E}[u_\ell\, u_\ell^*]$, $\mathbb{E}[u_k\, u_k^*]$ and $\mathbb{E}[u_\ell\, u_k^*]$. The derivations are provided in Appendix C, where it is shown that the variances read

$$\mathbb{E}[v_\ell\, v_\ell^*] = 2|\rho_\ell|^2\,\mathbb{E}[u_\ell\, u_\ell^*]^3, \tag{39}$$

$$\mathbb{E}[v_k\, v_k^*] = 2|\rho_k|^2\,\mathbb{E}[u_k\, u_k^*]^3. \tag{40}$$

In Appendix C, it is also shown that the covariance reads

$$\mathbb{E}[v_\ell\, v_k^*] = 2\rho_\ell\rho_k^*\,\mathbb{E}[u_\ell\, u_k^*]\;|\mathbb{E}[u_\ell\, u_k^*]|^2\,. \tag{41}$$

In (39)-(41), $\mathbb{E}[u_\ell\, u_\ell^*]$ is given (see, Appendix B) by (64), $\mathbb{E}[u_k\, u_k^*]$ by (65), and $\mathbb{E}[u_\ell\, u_k^*]$ by (66), respectively.

Based on (39)-(41), the variance $\mathbb{E}[d_\ell\, d_\ell^*]$ of the augmented distortion noise d_ℓ defined in (11) can be calculated. Inserting (39)-(41) into (17) yields

$$\begin{aligned}\mathbb{E}[d_\ell\, d_\ell^*] = 2|\rho_\ell|^2\mathbb{E}[u_\ell u_\ell^*]^3 &+ 4\,|\mathbb{E}[u_\ell\, u_k^*]|^2\,\Re[\,\mu_k^*\,\rho_\ell\rho_k^*\,\mathbb{E}[u_\ell\, u_k^*]] \\ &+ 2|\mu_k|^2\,|\rho_k|^2\,\mathbb{E}[u_k\, u_k^*]^3.\end{aligned} \tag{42}$$

The covariance $\mathbb{E}[d_\ell\, d_k^*]$ of the augmented distortion noise d_ℓ is calculated by the insertion of (39)-(41) into (26), that is

$$\begin{aligned}\mathbb{E}[d_\ell\, d_k^*] \;=\; & 2\rho_\ell\rho_k^*\,\mathbb{E}[u_\ell\, u_k^*]\;|\mathbb{E}[u_\ell\, u_k^*]|^2 \\ & + 2\mu_\ell^*\,|\rho_\ell|^2\,\mathbb{E}[u_\ell\, u_\ell^*]^3 + 2\mu_k\,|\rho_k|^2\,\mathbb{E}[u_k\, u_k^*]^3 \\ & + 2\mu_k\mu_\ell^*\,\rho_\ell^*\rho_k\,\mathbb{E}[u_\ell\, u_k^*]^*\;|\mathbb{E}[u_\ell\, u_k^*]|^2\,.\end{aligned} \tag{43}$$

$$\text{NMSE}_\ell = \frac{|\gamma_\ell(\alpha_\ell - 1) + \alpha_k\,\gamma_k\,\mu_k\,\delta_\ell + (\alpha_\ell\,\gamma_\ell\,\delta_k + \alpha_k\,\gamma_k\,\mu_k)\beta^*\xi^*|^2}{|\gamma_\ell|^2\,(1+|\xi|^2)} + \frac{|(\gamma_\ell(\alpha_\ell - 1) + \alpha_k\,\gamma_k\,\mu_k\,\delta_\ell)\xi + (\alpha_\ell\,\gamma_\ell\,\delta_k + \alpha_k\,\gamma_k\,\mu_k)\beta^*|^2}{|\gamma_\ell|^2\,(1+|\xi|^2)}$$
$$+ \frac{2|\rho_\ell|^2\,\mathbb{E}[u_\ell\,u_\ell^*]^3}{|\gamma_\ell|^2\,\sigma_x^2} + \frac{4\,|\mathbb{E}[u_\ell\,u_k^*]|^2\,\Re[\,\mu_k^*\,\rho_\ell\rho_k^*\,\mathbb{E}[u_\ell\,u_k^*]]}{|\gamma_\ell|^2\,\sigma_x^2} + \frac{2|\mu_k|^2\,|\rho_k|^2\,\mathbb{E}[u_k\,u_k^*]^3}{|\gamma_\ell|^2\,\sigma_x^2} + \frac{(1+|\mu_k|^2)\,\sigma_w^2}{|\gamma_\ell|^2\,\sigma_x^2}, \tag{44}$$

D. NMSE

The NMSE (16) as a function of the involved parameters is now summarized in (44), as shown at the top of this page. The derived expression for the NMSE includes the Bussgang attenuations $\{\alpha_\ell,\,\alpha_k\}$ in (37); the variances $\mathbb{E}[u_\ell\,u_\ell^*]$ and $\mathbb{E}[u_k\,u_k^*]$ in (64)-(65); and covariance $\mathbb{E}[u_\ell\,u_k^*]$ in (66). The expression (44) is clearly too cumbersome to interpret by visual inspection.

On average, the NMSE is independent of the correlation of the input streams. Accordingly, it is sufficient to study the case $\xi = 0$. For $\xi = 0$, the properties (64)-(66) of the inputs to the nonlinear functions are reduced to $\mathbb{E}[u_\ell\,u_\ell^*] = (1+|\delta_k|^2\,|\beta|^2)\,|\gamma_\ell|^2\sigma_x^2$, $\mathbb{E}[u_k\,u_k^*] = (|\beta|^2+|\delta_\ell|^2)\,|\gamma_k|^2\,\sigma_x^2$, and $\mathbb{E}[u_\ell\,u_k^*] = (\delta_\ell^* + |\beta|^2\delta_k)\,\gamma_\ell\,\gamma_k\,\sigma_x^2$, respectively. Now, the Bussgang attenuation (37) reads

$$\alpha_\ell = 1 + 2\rho_\ell\,(1+|\delta_k|^2\,|\beta|^2)\,|\gamma_\ell|^2\,\sigma_x^2. \tag{45}$$

The resulting NMSE is still a complicated function of the involved parameters and is considered beyond the scope of the paper.

For an almost ideal 3rd order system, (18) is applicable. Neglecting higher order terms $\Delta_\ell \simeq 2\rho_\ell\,|\gamma|^2\,\sigma_x^2$ and $\mathbb{E}[v_\ell\,v_\ell^*] \simeq 2|\rho_\ell|^2\,|\gamma|^6\,\sigma_x^6$. Then

$$\text{NMSE}_\ell \simeq 6|\rho_\ell|^2\,|\gamma|^4\,\sigma_x^4 + |\beta|^2\,|\delta_k+\mu_k|^2 + \frac{\sigma_w^2}{|\gamma|^2\,\sigma_x^2}. \tag{46}$$

The effect of crosstalk is clearly visible and is manifested by the floor level proportional to $|\delta_k+\mu_k|^2$. Note that if $\beta = 0$, higher order crosstalk will be visible in the NMSE, which are neglected in the derivation of (46).

E. SNDR

It is interesting to compare the NMSE in (46) with the signal-to-noise-and-distortion ratio (SNDR). From (11), the SNDR for uncorrelated streams reads

$$\text{SNDR}_\ell = \frac{|\gamma_\ell\alpha_\ell + \gamma_k\alpha_k\mu_k\delta_\ell|^2}{|\gamma_\ell\alpha_\ell\delta_k + \gamma_k\alpha_k\mu_k|^2 + \mathbb{E}[d_\ell d_\ell^*]/\sigma_x^2 + \mathbb{E}[n_\ell n_\ell^*]/\sigma_x^2}, \tag{47}$$

by employing the above approximations, that is inserting α_ℓ given by $\alpha_\ell \simeq 1 + 2\rho_\ell\,|\gamma|^2\,\sigma_x^2$, and $\mathbb{E}[d_\ell\,d_\ell^*] \simeq 2|\rho_\ell|^2\,|\gamma|^6\,\sigma_x^6$. This calculation provides a closed form expression for SNDR, and by neglecting the higher order terms the result reads

$$\text{SNDR}_\ell \simeq \frac{1}{2|\rho_\ell|^2\,|\gamma|^4\,\sigma_x^4 + |\delta_k+\mu_k|^2 + \sigma_w^2/|\gamma|^2\,\sigma_x^2}. \tag{48}$$

For both NMSE in (46) and the inverse of the SNDR in (48), it holds that their first term depends on the compression parameter ρ_ℓ, the second depends on the crosstalk via δ_k and μ_k, and the third term depends on the additive noise via its power σ_w^2.

F. NEC and Distortion Noise Covariance

A similar expression as for the NMSE in (44) can be obtained for the NEC in (25); however, this has been left out of the paper. Here, the approximate expression (27) is studied.

Consider two identical amplifiers (that is, $\rho = \rho_\ell = \rho_k$) without crosstalk, driven by correlated input streams of equal powers, that is $\mathbb{E}[u_\ell\,u_\ell^*] = \sigma_u^2$, $\mathbb{E}[u_k\,u_k^*] = \sigma_u^2$, and $\mathbb{E}[u_\ell\,u_k^*] = \theta_u\,\sigma_u^2$ for some given σ_u^2, where $\theta_u = |\theta_u|\,e^{j\phi}$ is the correlation coefficient, with $|\theta_u| \le 1$. From (39)-(40), the variance of the distortion noises reads $\mathbb{E}[v_\ell\,v_\ell^*] = \mathbb{E}[v_k\,v_k^*] = 2|\rho|^2\,\sigma_u^6$, and the covariance (41) reads

$$\mathbb{E}[v_\ell\,v_k^*] = 2|\rho|^2\,\theta_u\,|\theta_u|^2\sigma_u^6. \tag{49}$$

Now, the correlation coefficient θ_v of the distortion noise reads

$$\theta_v = \frac{\mathbb{E}[v_\ell\,v_k^*]}{2|\rho|^2\,\sigma_u^6} = |\theta_u|^3\,e^{j\phi}. \tag{50}$$

The relationship between the correlation coefficients is $\theta_v/\theta_u = |\theta_u|^2$, and thus the phase is preserved; however, the magnitude of the distortion noise is reduced when compared with the correlation of the input streams. The result above coincides with the result presented in [7], where it was concluded: *"The fact that the phase of the input is preserved in the distortion noise indicates that the spatial direction of the transmitted noise will be the same as that of the desired signal."* Since the magnitude of the correlation coefficient decays by the power of three, it is typically claimed that the correlation is small [10], [12], [30]. One should note that the results in [7] neither consider the thermal noise, nor the crosstalk.

Now, consider a linear reciprocal symmetric network (real-valued and equal values of the crosstalk parameters, and equal gains) with $\beta = 1$. Then σ_u^2 reads (c.f. (64), in the Appendix B)

$$\sigma_u^2 = \frac{|1+\delta\,\xi^*|^2 + |\xi+\delta|^2}{1+|\xi|^2}\,|\gamma|^2\,\sigma_x^2, \tag{51}$$

and the correlation coefficient follows, that is

$$\theta_u = \frac{2(1+\delta\,\xi^*)\,(\xi+\delta)}{|1+\delta\,\xi^*|^2 + |\xi+\delta|^2}. \tag{52}$$

For the case that the input crosstalk influences the correlation, that is for $|\xi| \approx \delta$ with $\xi = |\xi|\,e^{i\phi}$, it holds that $\theta_u \simeq 2(|\xi|\,e^{i\phi} + \delta)$. Accordingly, the input crosstalk bias the phase angle of the data stream and the distortion towards zero degrees. The output crosstalk determined by $\mu \in \mathbb{R}$ adds additional bias in the phase angle. A simulation example is included in Sec. VI.

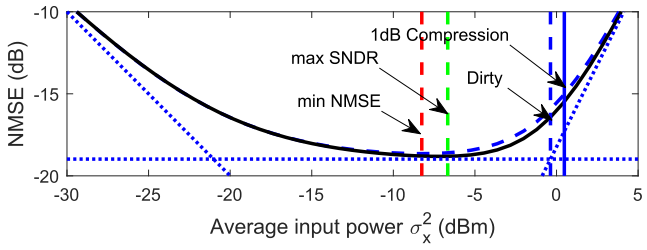

Fig. 3. Theoretical NMSE (44) (black solid line) and its approximation (46) (blue dashed line) versus average input power σ_x^2 at -25 dB crosstalk. The three asymptotes in (46) are included (dotted blue lines). The three vertical dashed lines indicate the back-offs (53) (leftmost, red), (54) (middle, green), and (55) (rightmost, blue), respectively. The solid vertical line (blue) indicates the 1dB compression point (33).

V. Power Back-Off Optimization and DPD

In this section, the optimization of the point of operation, that is the input power back-off, and dirty MIMO transmitters subject to DPD are considered.

A. Power Amplifier Back-Off Optimization

The NMSE floor provided by the term $|\delta_k + \mu_k|^2$ in (46) does not influence a minimization of the NMSE with respect to power amplifier back-off, thus *it can be concluded that power amplifier back-off optimization is, on average, independent of channel crosstalk.* However, the NMSE-minima broadens for increasing crosstalk, and thus sub-optimal schemes may be favorable, as will be discussed at the end of this section. First, however, optimal schemes are examined.

One can note that for this class of nonlinear systems, SNDR is not inversely proportional to the NMSE, meaning that a different input back-off power σ_x^2 is obtained when minimizing NMSE, compared to when maximizing SNDR. Starting with the approximate expression for the NMSE in (46), note that the minimum NMSE is obtained at

$$\sigma_x^2 = \arg\min_{\sigma_x^2} \text{NMSE} = \frac{1}{|\gamma|^2} \sqrt[3]{\frac{\sigma_w^2}{12|\rho_\ell|^2}}. \tag{53}$$

In a first approximation (53) is independent of the leakage or properties of the adjacent channel. Note also that the SNDR in (48) is maximized for a slightly higher input power, that is

$$\sigma_x^2 = \arg\max_{\sigma_x^2} \text{SNDR} = \frac{1}{|\gamma|^2} \sqrt[3]{\frac{\sigma_w^2}{4|\rho_\ell|^2}}. \tag{54}$$

Thus, maximizing SNDR over minimizing NMSE allows for an 1.6 dB increased input power level; that enables a more energy efficient operation of the power amplifier.

For MIMO-transmitters subject to crosstalk, the average input power can be further increased, subject to a small increase in NMSE. This is evident from Fig. 3, which displays the NMSE for a slightly nonlinear transmitter subjected to -25 dB crosstalk. See the numerical examples in Sec. VI for further details on parameter settings. Taking the vertex between the asymptotes defined by the first and second terms of (46) as the objective function yields

$$\sigma_x^2 = \frac{1}{|\gamma|^2} \frac{|\beta|\,|\delta_k + \mu_k|}{\sqrt{6}\,|\rho_\ell|}. \tag{55}$$

Here, one can note that (55) is determined by the leakage, amplifier gain, and nonlinear compression ρ_ℓ, but is independent of the in-channel noise. Using the power amplifier back-off (55) over minimizing NMSE allows, in the given example in Fig. 3, for an 8 dB increased input power level, subject to an NMSE 3 dB above the minimum NMSE.

B. 2×2 Dirty MIMO Subject to DPD

In this section, the dirty 2×2 MIMO transmitter is subject to DPD as described e.g. in [16], in which case Stage 2 in Fig. 1 is replaced by a unit that predistorts the streams. Accordingly, a 2×2 power amplifier subject to *ideal DPD* is modeled as a soft limiter

$$r_\ell = \begin{cases} u_\ell, & |u_\ell| \le A \\ A\, e^{j\angle u_\ell}, & |u_\ell| > A \end{cases}, \tag{56}$$

with $A \in \mathbb{R}$ being a clipping level to be determined. A perfectly linearized transmitter is also without crosstalk, that is $\delta_k \approx 0$ and $\mu_k \approx 0$.

The clipping level A in (56) depends on the normalization gain used in the linearization [29]. All terms in the resulting NMSE are affected by the normalization gain that is used. For the sake of the discussion, here the third order model (28) is subject to the DPD preserving the small signal unity gain of $f_\ell(\cdot)$, and it is assumed that the original amplifier can be operated up to an X-dB compression point. Then, the clipping level A is given by (cf. (32))

$$A^2 = \frac{1}{3|\rho_\ell|}\left(1 - \frac{\sqrt{-1 + 3\cdot 10^{-X/10}}}{\sqrt{2}}\right) = \frac{C_{X\text{dB}}}{|\rho_\ell|}, \tag{57}$$

where $C_{X\text{dB}} \approx \{0.056, 0.11, 0.17\}$ for $X = 1, 2, 3$ (dB) respectively. The normalization gain and clipping level used in the linearization are related. For a monotonically decreasing nonlinearity, the 0 dB small signal gain has the highest normalization gain versus power. The clipping level in (57) is the lowest clipping level.

The NMSE for the SISO system (56) is given by, cf. [34]

$$\text{NMSE} = e^{-\eta^2} - 2\eta\sqrt{\pi}\,Q(\sqrt{2\eta^2}) + \frac{\sigma_w^2}{|\gamma|^2\,\sigma_x^2}, \tag{58}$$

where $Q(\cdot)$ denotes the tail probability of the standard normal distribution and where $\eta^2 = A^2/(|\gamma|^2\,\sigma_x^2)$. To emphasize that a SISO model is studied, the subscript ℓ is dropped in the NMSE.

The generic results derived in (18) are applied to study the effects of residual crosstalk due to imperfect DPD. As shown in Appendix E, $\Delta_\ell = \alpha_\ell - 1$ reads $\Delta_\ell = -e^{-\eta_\ell^2}/2$, and

$$\mathbb{E}[v_\ell\, v_\ell^*] = \frac{|\gamma|^4\, e^{-\eta^2}\,\sigma_x^4}{2A^2}, \tag{59}$$

where $\eta^2 \simeq A^2/(|\gamma|^2\,\sigma_x^2)$. Summing up and reordering the terms in (18) gives

$$\text{NMSE}_\ell \simeq \frac{|\gamma|^2\, e^{-\eta^2}\,\sigma_x^2}{2A^2} + |\beta|^2\,|\delta_k + \mu_k|^2 + \frac{\sigma_w^2}{|\gamma|^2\,\sigma_x^2}, \tag{60}$$

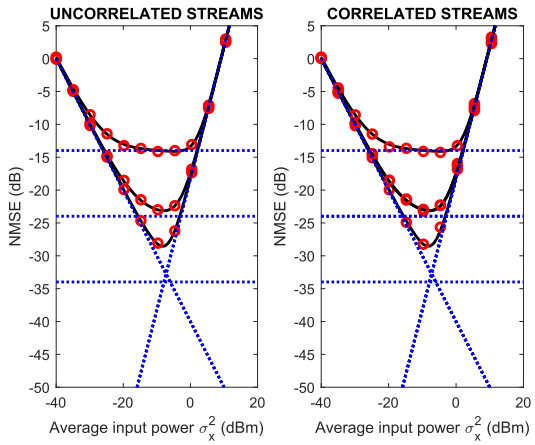

Fig. 4. Theoretical NMSE (44) versus average input power σ_x^2 for uncorrelated input streams (left figure, $\xi = 0$), and correlated input streams (right figure, $\xi = e^{i\Phi}$, where Φ in randomly drawn from $\mathcal{U}[-\pi, \pi]$). The three asymptotes for the approximate expression for NMSE in (46) are included (dashed blue line), for varying leakage (-20, -30, and -40 dB respectively). Simulation results are indicated by red circles.

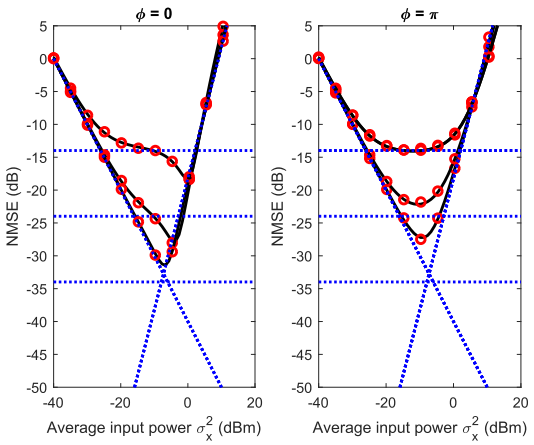

Fig. 5. Theoretical NMSE (44) versus average input power σ_x^2 for correlated input streams with fixed phase (left figure, $\xi = 1$, and right figure, $\xi = e^{i\pi} = -1$). The three asymptotes for the approximate expression for NMSE in (46) (dashed black line), for varying leakage (-20, -30, and -40 dB respectively). Simulation results are indicated by red circles.

where the term $|\Delta_\ell|^2$ in (18) was neglected. The result (60) is a generalization of the approximate SISO-result derived in [31], with the included effects of MIMO-channel crosstalk. Again, the NMSE floor provided by the term $|\delta_k + \mu_k|^2$ in (60) does not influence the minimization of the NMSE with respect to the power amplifier back-off. Accordingly, a closed-form expression for the optimal back-off minimizing NMSE is known to be [34]

$$\sigma_u^2 \simeq \frac{A^2}{W\left(A^2/2\sigma_w^2\right)}, \tag{61}$$

where $W(\cdot)$ is the Lambert-W function [32]. Accordingly, employing $\sigma_u^2 \simeq |\gamma|^2\, \sigma_x^2$, cf. (64), the back-off reads

$$\sigma_x^2 \simeq \frac{1}{|\gamma|^2} \frac{A^2}{\ln(A^2/2\sigma_w^2) - \ln(\ln(A^2/2\sigma_w^2))}, \tag{62}$$

where the approximation $W(x) \approx \ln(x) - \ln(\ln(x))$ was used, with $\ln(\cdot)$ being the natural logarithm. One can note that, as with (57), the back-off is a function of the undistorted amplifier properties via $C_{X\text{dB}}$, γ and ρ_ℓ, as well as the thermal noise via σ_w^2.

VI. Numerical Examples

A. NMSE for Uncorrelated and Correlated Input Streams

In the first example, a set-up with $\{-20, -30, -40\}$ dB crosstalk is considered, that is when $\{\delta_\ell, \delta_k, \mu_\ell, \mu_k\}$ are all real-valued quantities of equal value δ, and where the crosstalk in dB is given by $20\log_{10}\delta$. The compression parameter of the power amplifiers is given by $\rho = \rho_\ell = \rho_k = -0.05$. The nominal gain $\gamma = 30$ dB, with perfectly balanced branches, that is $\gamma_\ell = \gamma_k = \gamma$. The variance of the thermal noise is $\sigma_v^2 = 10^{-4}$, or -10 dBm. The stage 2 gain β is given by $\beta = 1$. According to (53), the average input power minimizing NMSE is given by $\sigma_x^2 = -8.2$ dBm.

In Fig. 4, the theoretical NMSE (44) is calculated and compared with the result based on numerical Matlab simulations which were based on $N = 1,000$ independently drawn Gaussian samples. An excellent agreement was noted when the theoretical predictions and the simulation results were compared. Further, the asymptotes individually and accurately bound the NMSE in the different regions of average input power. In Fig. 4–left, the input streams are uncorrelated of equal power, that is $\xi = 0$. In Fig. 4–right, the input streams are fully correlated, that is $\xi = e^{j\Phi}$, where Φ is for each sample drawn from a uniform distribution $\mathcal{U}[-\pi, \pi]$. The theoretical NMSE shown in Fig. 4–right is the one that corresponds to the uncorrelated input streams.

B. NMSE for Given Correlation Phase Angle

The simulations in Sec. VI-A are repeated for two fixed phase angles (that is, best and worse case) of ξ, that is $\xi = e^{j\phi}$ where $\phi = 0$, or $\phi = \pi$ respectively. The results are displayed in Fig. 5, together with the theoretical predictions of NMSE given by (44).

The term T in (21) obtains its largest negative value for $\phi = 0$, and its largest positive value for $\phi = \pi$. Since T is proportional to σ_x^2, the influence of T on the total NMSE increases with increasing input power σ_x^2, which explains the non-symmetrical curves in Fig. 5.

C. NEC and Distortion Noise Covariance

In Fig. 6, the relative phase angle of NEC (25) (relative to the angle ϕ of the correlation coefficient $\xi = e^{j\phi}$) is studied as a function of the additive noise and crosstalk, with parameter settings, as in the previous examples. The ideal noise-free and crosstalk-free case is displayed in the upper left diagram of Fig. 6. Here, the $N = 1,000$ drawn samples are divided into ten blocks, with one block of data used per simulation run. Fig. 6 shows the ten overlaid results, indicating the spread of the phase angle at low signal to noise ratios. The additive noise provides an almost uniform spread of the phase angle up to the point of optimal back-off (53), after which the phase angle of (25) is well-centered around ϕ, as expected. The crosstalk

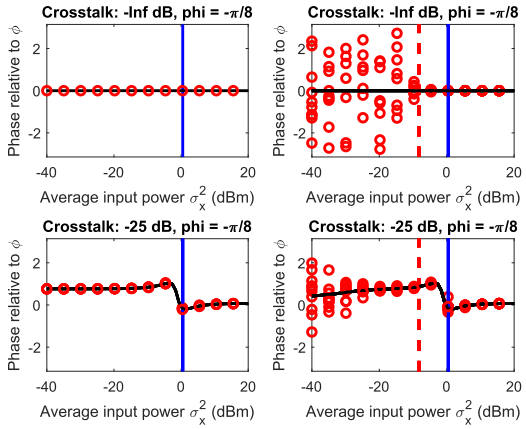

Fig. 6. Theoretical phase angle of NEC (25) (solid black line) relative the phase angle of $\xi = e^{j\phi}$ for $\phi = -\pi/8$. Left plots with $\sigma_w^2 = 0$, and right plots with $\sigma_w^2 = -10$ dBm. Ten overlaid simulations, each based on 100 drawn samples. The two vertical lines indicate the NMSE-optimal back-off (53) (red dashed line), the 1dB compression point (33) (blue solid line). Simulation results are indicated by red circles.

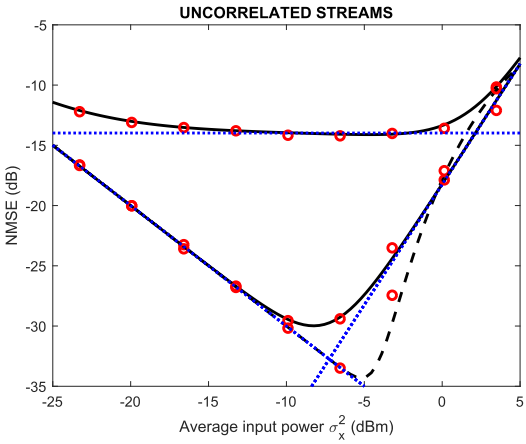

Fig. 7. NMSE (44) (solid black lines) and NMSE for ideal DPD (58) (dashed black line), versus average input power σ_x^2, for $\{-20, -\infty\}$ dB crosstalk. The three asymptotes in (46) (dashed blue lines) are included. Simulation results (red circles).

(lower left figure in Fig. 6) distorts the phase angle in a quite complicated manner. In the considered example, the shift in phase occurs at the 1dB compression point. However, other settings provide other locations of the phase shift. Finally, the effect of both additive noise and crosstalk is considered, indicating that the crosstalk somewhat concentrates the spatial direction of the transmitted noise.

D. Effects of DPD

Fig. 7 illustrates the effect of DPD on the NMSE versus input power. Here, the common compression parameter $\rho = -0.05$ and the crosstalk is -20 dB, and $-\infty$ dB respectively. The NMSE results are shown for the uncompensated transmitter with and without crosstalk, together with the NMSE for a transmitter subjected to ideal DPD. The clipping level A is given by $C_{3\text{dB}}$ in (57). Uncorrelated input streams are considered, that is $\xi = 0$.

It should be noted that a different choice of normalization gain could affect the asymptotes. A smaller normalization gain and correspondingly higher clipping level would give a higher level of the asymptote $\propto 1/\sigma_x^2$ and a lower level than of that $\propto \sigma_x^4$ in Fig. 7.

Ideal DPD pushes down the achievable NMSE as well as pushing up in power the optimal (minimum NMSE) back-off, from -8.3 dBm given by (53), to -5.1 dBm given by (62), that is around a 3 dB improvement.

VII. Conclusions

The performance of a dirty 2×2 MIMO transmitter has been studied. The figures of merit such as NMSE and NEC are quite complicated functions of the crosstalk, amplifier nonlinearity, and the correlation of the input streams, as illustrated by the NMSE in (44) for a 2×2 MIMO transmitter subject to third order nonlinear distortion which mimics a solid state transmitter.

A third order nonlinear model was studied in detail in the MIMO context, and included a 1-dB compression point, signal dependent compression, the relationship between NMSE and SNDR, and different schemes to determine the power amplifier back-off. Besides a detailed study of the NMSE, the covariance of the distortion noise was investigated. Through a more streamlined derivation than the one in the original work [7], the correlation coefficient of the distortion noise was derived and revealed the preservation of the phase angle and the third order decay in magnitude.

Approximate expressions for the NMSE have been derived and the higher order terms in these expressions have been discarded, and thereby revealing the asymptotes reflecting the influence of thermal noise, crosstalk, and nonlinear compression respectively. The paper includes (18) and (19) for generic nonlinear functions, (46) for third order nonlinearities which reflects a solid state amplifier, and (60) for MIMO-systems subject to ideal DPD.

The approximate NMSE expression derived for generic nonlinearities in (18) and (19) revealed that, on average, the NMSE is independent of the correlation of the input streams. Equations (18) and (19) also show that for specific input streams, the NMSE is dependent on the correlation between the input OFDM streams. Accordingly, improvement or degradation of the NMSE over the NMSE for uncorrelated streams can be obtained in specific scenarios, e.g. streams under beamforming or linear precoding. The NMSE improvement is, however, bounded by the NMSE of a crosstalk-free MIMO transmitter.

The expressions for the NMSE show a characteristic behavior when the transmitter is subject to crosstalk, in that they are manifested by a lower bound on the NMSE that is independent of the input power. Accordingly, the crosstalk does not influence the value of the input power that provides minimum NMSE. The independence of NMSE on the input correlation and channel crosstalk implies that power amplifier back-off optimization for a SISO transmitter is also directly applicable to the dirty MIMO transmitter. However, as shown in e.g. Fig. 3, the above results should be handled with care,

since it is also shown that the crosstalk significantly broadens the shape of the NMSE around its minimum. This observation opens up for novel sub-optimal schemes for power amplifier back-off determination, where (as opposite to the crosstalk-free case with a quite narrow minimum) a substantial increase in input power can be traded against a small increase in NMSE. Such a novel crosstalk tailored back-off scheme was proposed in (55).

The result in [7] on the properties of the distortion noise are extended to dirty MIMO channels subject to crosstalk. It is shown that, in the small signal region, the thermal noise typically uniformly spreads the spatial direction of the transmitted noise. However, the effect of crosstalk is a concentration in the spatial direction. This finding provides support to the simplified transmission model used in e.g. [9]–[12].

Finally, to reflect on the question proposed in the title of this paper. In comparison with a SISO transmitter, the MIMO transmitter is subject to channel crosstalk and the possible correlation of the input streams. On average, the input stream correlation does not deteriorate the NMSE, but the crosstalk does. MIMO crosstalk will always reduce the performance in terms of NMSE, compared with the performance of the SISO channel. In fact, consider the ℓ:th channel in a dirty MIMO transmitter operating under optimal (that is, minimizing NMSE) back-off, that is subject to $\delta_k+\mu_k$ adjacent channel crosstalk. The ℓ:th channel performs like an equivalent SISO transmitter with a signal-to-noise ratio

$$\mathrm{SNR}_\ell \triangleq \frac{|\gamma|^2\,\sigma_x^2}{\sigma_w^2} = \frac{3}{2|\delta_k+\mu_k|^2}. \tag{63}$$

See Appendix D for details on the derivation of (63). Accordingly, the question "*Dirty MIMO transmitters: does it matter?*" can be rephrased as "*Is the SNR (63) of the equivalent SISO transmitter good enough?*", since a decoupled simplified transmission model can be formulated. The channel distortion noises can be handled as uncorrelated. The correlation of the input streams does not influence performance.

APPENDIX

INPUT STREAMS AND INPUT CROSSTALK

A. Properties of Correlated Input Streams $\{x_\ell,\, x_k\}$

Consider the two streams (5) and (6), where $\{\tilde{x}_\ell,\, \tilde{x}_k\}$ are jointly uncorrelated white Gaussian noise sources, both with variance $\sigma_{\tilde{x}}^2 = \mathbb{E}[\tilde{x}_\ell\,\tilde{x}_\ell]$, and where ξ determines the correlation between the streams. Let $\sigma_{\tilde{x}}^2 = \sigma_x^2/(1+|\xi|^2)$. Then, the average power of x_ℓ equals σ_x^2, independently of the value of the cross-correlation parameter ξ, that is $\mathbb{E}[x_\ell\,x_\ell^*] = (1+|\xi|^2)\,\sigma_{\tilde{x}}^2 = \sigma_x^2$. In a similar vein, $\mathbb{E}[x_k\,x_k^*] = |\beta|^2\,\sigma_x^2$. Finally, the covariance $\mathbb{E}[x_\ell\,x_k^*]$ reads

$$\mathbb{E}[x_\ell\,x_k^*] = \mathbb{E}[(\tilde{x}_\ell+\xi\,\tilde{x}_k)\beta(\tilde{x}_k^*+\xi\,\tilde{x}_\ell^*)] = \frac{2\xi\,\beta}{1+|\xi|^2}\,\sigma_x^2,$$

with $\mathbb{E}[x_k\,x_\ell^*] = \mathbb{E}[x_\ell\,x_k^*]^*$.

B. Properties of the Nonlinearity Excitations $\{u_\ell,\, u_k\}$

The input $p_\ell = x_\ell + \delta_k\,x_k$ in (4) reads

$$\begin{aligned} p_\ell &= \tilde{x}_\ell + \xi\,\tilde{x}_k + \delta_k\,\beta^*(\tilde{x}_k + \xi^*\,\tilde{x}_\ell) \\ &= (1+\delta_k\,\beta^*\,\xi^*)\tilde{x}_\ell + (\xi+\delta_k\beta^*)\,\tilde{x}_k, \end{aligned}$$

where (5)-(6) were used in the first equality. In a similar vein, the input $p_k = x_k + \delta_\ell\,x_\ell$ reads

$$\begin{aligned} p_k &= \beta^*(\tilde{x}_k + \xi^*\,\tilde{x}_\ell) + \delta_\ell\,(\tilde{x}_\ell + \xi\,\tilde{x}_k) \\ &= (\beta^*+\delta_\ell\,\xi)\tilde{x}_k + (\beta^*\xi^*+\delta_\ell)\,\tilde{x}_\ell. \end{aligned}$$

With $u_\ell = \gamma_\ell\,p_\ell$ and $u_k = \gamma_k\,p_k$, the variance $\mathbb{E}[u_\ell\,u_\ell^*]$ of the ℓ:th channel reads

$$\mathbb{E}[u_\ell\,u_\ell^*] = \frac{|1+\delta_k\,\beta^*\,\xi^*|^2 + |\xi+\delta_k\,\beta^*|^2}{1+|\xi|^2}\,|\gamma_\ell|^2\,\sigma_x^2. \tag{64}$$

The variance $\mathbb{E}[u_k\,u_k^*]$ of the k:th channel equals

$$\mathbb{E}[u_k\,u_k^*] = \frac{|\beta^*+\delta_\ell\,\xi|^2 + |\beta^*\,\xi^*+\delta_\ell|^2}{1+|\xi|^2}\,|\gamma_k|^2\,\sigma_x^2. \tag{65}$$

The covariance $\mathbb{E}[u_\ell\,u_k^*]$ is given by

$$\mathbb{E}[u_\ell u_k^*] = \frac{(1+\delta_k\beta^*\xi^*)(\beta\xi+\delta_\ell^*) + (\beta+\delta_\ell^*\xi^*)(\xi+\delta_k\beta^*)}{1+|\xi|^2} \times\gamma_\ell\gamma_k^*\sigma_x^2, \tag{66}$$

with $\mathbb{E}[u_k\,u_\ell^*] = \mathbb{E}[u_\ell\,u_k^*]^*$.

THIRD ORDER NONLINEAR SYSTEMS

C. Properties of the Distortion Noise $\{v_\ell, v_k\}$

1) Distortion Noise is Zero-Mean: It is clear that the distortion noise (38) is zero-mean, that is

$$\mathbb{E}[v_\ell] = \rho_\ell\,\mathbb{E}[u_\ell\,|u_\ell|^2] - 2\rho_\ell\,\mathbb{E}[u_\ell]\,\mathbb{E}[u_\ell\,u_\ell^*] = 0,$$

where odd order central moments of a complex Gaussian stochastic variable equal zero were used.

2) The Variance $\mathbb{E}[v_\ell\,v_\ell^*]$: With the distortion noise (38) as the starting point, a straightforward calculation gives

$$\begin{aligned} \frac{\mathbb{E}[v_\ell v_\ell^*]}{|\rho_\ell|^2} &= \mathbb{E}\left[u_\ell u_\ell^*(|u_\ell|^2 - 2\mathbb{E}[u_\ell u_\ell^*])^2\right] \\ &= \mathbb{E}[(u_\ell u_\ell^*)^3] + 4\mathbb{E}[u_\ell u_\ell^*]^3 - 4\mathbb{E}[u_\ell u_\ell^*]\mathbb{E}[(u_\ell u_\ell^*)^2]. \end{aligned}$$

Using the relations for complex Gaussian stochastic variables $\mathbb{E}[(u_\ell\,u_k^*)^3] = 6\,\mathbb{E}[u_\ell\,u_k^*]^3$, and $\mathbb{E}[(u_\ell\,u_k^*)^2] = 2\,\mathbb{E}[u_\ell\,u_k^*]^2$, then a straightforward calculation yields (39). In a similar vein, (40) follows.

3) The Covariance $\mathbb{E}[v_\ell\,v_k^*]$: To calculate the covariance $\mathbb{E}[v_\ell\,v_k^*]$, first note from (38) that

$$\frac{\mathbb{E}[v_\ell v_k^*]}{\rho_\ell\rho_k^*} = \mathbb{E}\left[u_\ell u_k^*(|u_\ell|^2 - 2\mathbb{E}[u_\ell u_\ell^*])(|u_k|^2 - 2\mathbb{E}[u_k u_k^*])\right].$$

Resolving the product yields

$$\begin{aligned} \frac{\mathbb{E}[v_\ell v_k^*]}{\rho_\ell\rho_k^*} &= \mathbb{E}[(u_\ell u_k^*)^2(u_\ell u_k^*)^*] + 4\mathbb{E}[u_\ell u_\ell^*]\mathbb{E}[u_k u_k^*]\mathbb{E}[u_\ell u_k^*] \\ &\quad -2\mathbb{E}[u_\ell u_\ell^*]\mathbb{E}[u_\ell u_k^*|u_k|^2] - 2\mathbb{E}[u_k u_k^*]\mathbb{E}[u_\ell u_k^*|u_\ell|^2]. \end{aligned}$$

Now, using the result (67) derived in Appendix E, and the relations $\mathbb{E}[u_\ell\,u_k^*\,|u_k|^2] = 2\,\mathbb{E}[u_k\,u_k^*]\,\mathbb{E}[u_\ell\,u_k^*]$ and $\mathbb{E}[u_\ell\,u_k^*\,|u_\ell|^2] = 2\,\mathbb{E}[u_\ell\,u_\ell^*]\,\mathbb{E}[u_\ell\,u_k^*]$ [28], then a straightforward calculation yields (41).

4) The Cross Covariance $\mathbb{E}[v_\ell\, u_k^*]$*:* By construction, the distortion noise is uncorrelated with the amplifier output $s_\ell = \alpha_\ell\, u_\ell$ since $\mathbb{E}[v_\ell\, u_\ell^*] = 0$. Further, $\mathbb{E}[v_\ell\, u_k^*] = 0$, as shown below

$$\begin{aligned}\mathbb{E}[v_\ell\, u_k^*] &= \mathbb{E}[\rho_\ell\, u_\ell\, (|u_\ell|^2 - 2\,\mathbb{E}[u_\ell\, u_\ell^*])\, u_k^*] \\ &= \rho_\ell\, \mathbb{E}[u_\ell\, u_k^* |u_\ell|^2] - 2\rho_\ell\, \mathbb{E}[u_\ell\, u_k^*]\, \mathbb{E}[u_\ell\, u_\ell^*] \\ &= 2\rho_\ell\, \mathbb{E}[u_\ell\, u_\ell^*]\, \mathbb{E}[u_\ell\, u_k^*] - 2\rho_\ell\, \mathbb{E}[u_\ell\, u_k^*]\, \mathbb{E}[u_\ell\, u_\ell^*] = 0.\end{aligned}$$

D. Equivalent SISO-Model

Consider a transmitter described by the third order nonlinearity (28) which operate at minimum-NMSE back-off, that is under the average input power given by (53). The corresponding minimum-NMSE is given by

$$\text{NMSE}_\ell \simeq \frac{3\sigma_w^2}{2|\gamma|^2\, \sigma_x^2}.$$

According to (46) (see also, e.g. Fig. 4), a significant amount of crosstalk results in an NMSE close to (for $\beta = 1$) $\text{NMSE}_\ell \simeq |\delta_k + \mu_k|^2$. The stated conclusion follows.

A Useful Result for Complex Gaussian Variables

E. A Result for 6th Order Moment of Gaussian Variables

To calculate the sixth order moment $\mathbb{E}[(u_\ell\, u_k^*)^2 (u_\ell\, u_k^*)^*]$, note that $\mathbb{E}[z_1\, z_2\, z_3\, z_4^*\, z_5^*\, z_6^*] = \sum_{t=1}^{6}\, T_t$, where [28]

$$\begin{aligned}T_1 &= \mathbb{E}[z_1\, z_4^*]\, \mathbb{E}[z_2\, z_5^*]\, \mathbb{E}[z_3\, z_6^*], \\ T_2 &= \mathbb{E}[z_1\, z_5^*]\, \mathbb{E}[z_2\, z_6^*]\, \mathbb{E}[z_3\, z_4^*], \\ T_3 &= \mathbb{E}[z_1\, z_6^*]\, \mathbb{E}[z_2\, z_4^*]\, \mathbb{E}[z_3\, z_5^*], \\ T_4 &= \mathbb{E}[z_1\, z_4^*]\, \mathbb{E}[z_2\, z_6^*]\, \mathbb{E}[z_3\, z_5^*], \\ T_5 &= \mathbb{E}[z_1\, z_5^*]\, \mathbb{E}[z_2\, z_4^*]\, \mathbb{E}[z_3\, z_6^*], \\ T_6 &= \mathbb{E}[z_1\, z_6^*]\, \mathbb{E}[z_2\, z_5^*]\, \mathbb{E}[z_3\, z_4^*].\end{aligned}$$

Let $z_1 = u_\ell$, $z_2 = u_\ell$, $z_3 = u_k$, $z_4 = u_k$, $z_5 = u_k$, and $z_6 = u_\ell$, then $T_1 = T_5 = \mathbb{E}[u_\ell\, u_k^*]^2\, \mathbb{E}[u_\ell\, u_k^*]^*$, and $T_2 = T_3 = T_4 = T_6 = E[u_\ell\, u_k^*]\, \mathbb{E}[u_\ell\, u_\ell^*]\, \mathbb{E}[u_k\, u_k^*]$. Accordingly, $\mathbb{E}[(u_\ell\, u_k^*)^2 (u_\ell\, u_k^*)^*] = 4\; T_2 + 2\; T_1$, or

$$\begin{aligned}&\mathbb{E}[(u_\ell\, u_k^*)^2 (u_\ell\, u_k^*)^*] \\ &\quad = 4\mathbb{E}[u_\ell\, u_k^*]\, \mathbb{E}[u_\ell\, u_\ell^*]\, \mathbb{E}[u_k\, u_k^*] + 2\mathbb{E}[u_\ell\, u_k^*]^2\, \mathbb{E}[u_\ell\, u_k^*]^*.\end{aligned} \tag{67}$$

Systems Subject to DPD

F. The Soft Limiter

For a model subject to crosstalk, the model loses its symmetry. Here, the ℓ:th channel is studied.

1) Bussgang Attenuation: The Bussgang attenuation reads [35]

$$\alpha_\ell = 1 - e^{-\eta_\ell^2} + \eta_\ell\, \sqrt{\pi}\, Q\left(\sqrt{2\eta_\ell^2}\right).$$

By construction, $\alpha_\ell \in \mathbb{R}$. Here, the input back-off level η_ℓ^2 is introduced as $\eta_\ell^2 = A_\ell^2/\sigma_u^2$, where

$$\sigma_u^2 = \mathbb{E}[u_\ell\, u_\ell^*] = (1 + |\delta_k\, \beta^*|^2)\, |\gamma|^2\, \sigma_x^2 \simeq |\gamma|^2\, \sigma_x^2,$$

where the second equality follows from (64) (for $\xi = 0$, because the average behavior is studied). Now, $\Delta_\ell = \alpha_\ell - 1$ reads

$$\Delta_\ell = -e^{-\eta_\ell^2} + \eta_\ell\, \sqrt{\pi}\, Q\left(\sqrt{2\eta_\ell^2}\right) \simeq -\frac{e^{-\eta_\ell^2}}{2},$$

where the approximation $\eta_\ell\, \sqrt{\pi}\, Q(\sqrt{2\eta_\ell^2}) \simeq e^{-\eta_\ell^2}/2$ [33] was used in the second equality.

2) Distortion Error: The variance of the distortion error $v_\ell = r_\ell - \alpha_\ell\, u_\ell$ reads [34]

$$\mathbb{E}[v_\ell\, v_\ell^*] = \left(1 - e^{-\eta_\ell^2} - \alpha_\ell^2\right) \sigma_u^2 \simeq \frac{e^{-\eta_\ell^2}\, \sigma_u^2}{2\eta_\ell^2},$$

where the following results were used in the second equality [31]

$$\alpha_\ell^2 \simeq \left(1 - \frac{e^{-\eta_\ell^2}}{2} - \frac{e^{-\eta_\ell^2}}{4\eta_\ell^2}\right)^2 \simeq 1 - e^{-\eta_\ell^2} - \frac{e^{-\eta_\ell^2}}{2\eta_\ell^2}.$$

Accordingly, $\mathbb{E}[v_\ell\, v_\ell^*] \simeq \sigma_u^4\, e^{-\eta^2}/2\; A^2$, where $\eta^2 = A^2/\sigma_u^2$ with A being the nominal clipping. The covariance of the distortion error in (59) follows.

References

[1] G. Fettweis, M. Löhning, D. Petrovic, M. Windisch, P. Zillmann, and W. Rave, "Dirty RF: A new paradigm," *Int. J. Wireless Inf. Netw.*, vol. 14, no. 2, pp. 133–148, Jun. 2007.

[2] R. Baum, "The correlation function of smoothly limited Gaussian noise," *IRE Trans. Inf. Theory*, vol. 3, no. 3, pp. 193–197, Sep. 1957.

[3] R. Price, "A useful theorem for nonlinear devices having Gaussian inputs," *IRE Trans. Inf. Theory*, vol. 4, no. 2, pp. 69–72, Jun. 1958.

[4] E. Costa, M. Midrio, and S. Pupolin, "Impact of amplifier nonlinearities on OFDM transmission system performance," *IEEE Commun. Lett.*, vol. 3, no. 2, pp. 37–39, Feb. 1999.

[5] C. H. A. Tavares, J. C. M. Filho, C. M. Panazio, and T. Abrão, "Input back-off optimization in OFDM systems under ideal pre-distorters," *IEEE Wireless Commun. Lett.*, vol. 5, no. 5, pp. 464–467, Oct. 2016.

[6] C. Studer, M. Wenk, and A. Burg, "MIMO transmission with residual transmit-RF impairments," in *Proc. Int. ITG Workshop Smart Antennas (WSA)*, Bremen, Germany, 2010, pp. 189–196.

[7] N. M. Moghadam, P. Zetterberg, P. Händel, and H. Hjalmarsson, "Correlation of distortion noise between the branches of MIMO transmit antennas," in *Proc. 23rd Annu. IEEE Int. Symp. Pers., Indoor Mobile Radio Commun. (PIMRC)*, Sydney, NSW, Australia, Sep. 2012, pp. 2079–2084.

[8] P. Zetterberg and N. Moghadam, "An experimental investigation of SIMO, MIMO, interference-alignment (IA) and coordinated multi-point (CoMP)," in *Proc. Int. Conf. Syst., Signals Image Process.*, Vienna, Austria, Apr. 2012, pp. 211–216.

[9] E. Björnson and E. Jorswieck, "Optimal resource allocation in coordinated multi-cell systems," *Found. Trends Commun. Inf. Theory*, vol. 9, nos. 2–3, pp. 113–381, 2013.

[10] E. Björnson, J. Hoydis, M. Kountouris, and M. Debbah, "Massive MIMO systems with non-ideal hardware: Energy efficiency, estimation, and capacity limits," *IEEE Trans. Inf. Theory*, vol. 60, no. 11, pp. 7112–7139, Nov. 2014.

[11] O. Elijah, C. Y. Leow, T. A. Rahman, S. Nunoo, and S. Z. Iliya, "A comprehensive survey of pilot contamination in massive MIMO—5G system," *IEEE Commun. Surveys Tuts.*, vol. 18, no. 2, pp. 905–923, 2nd Quart., 2016.

[12] E. Björnson, J. Hoydis, and L. Sanguinetti, "Massive MIMO networks: Spectral, energy, and hardware efficiency," *Found. Trends Signal Process.*, vol. 11, nos. 3–4, pp. 154–655, 2017.

[13] U. Gustavsson *et al.*, "On the impact of hardware impairments on massive MIMO," in *Proc. Globecom Workshops (GC Wkshps)*, 2014, pp. 294–300.

[14] Y. Zou *et al.*, "Impact of power amplifier nonlinearities in multi-user massive MIMO downlink," in *Proc. IEEE Globecom Workshops (GC Wkshps)*, San Diego, CA, USA, Dec. 2015, pp. 1–7.

[15] Y. Palaskas *et al.*, "A 5-GHz 108-Mb/s 2 × 2 MIMO transceiver RFIC with fully integrated 20.5-dBm P1dB power amplifiers in 90-nm CMOS," *IEEE J. Solid-State Circuits*, vol. 41, no. 12, pp. 2746–2756, Dec. 2006.
[16] S. Amin, P. N. Landin, P. Händel, and D. Rönnow, "Behavioral modeling and linearization of crosstalk and memory effects in RF MIMO transmitters," *IEEE Trans. Microw. Theory Techn.*, vol. 62, no. 4, pp. 810–823, Apr. 2014.
[17] H. Qian, X. Cheng, X. Luo, and W. Feng, "Calibration of nonlinear crosstalk in MIMO transmitter," *IEEE Trans. Veh. Technol.*, vol. 66, no. 5, pp. 3739–3748, May 2017.
[18] A. Vaezi, A. Abdipour, A. Mohammadi, and F. M. Ghannouchi, "On the modeling and compensation of backward crosstalk in MIMO transmitters," *IEEE Microw. Wireless Compon. Lett.*, vol. 27, no. 9, pp. 842–844, Sep. 2017.
[19] A. Abdelhafiz, L. Behjat, F. M. Ghannouchi, M. Helaoui, and O. Hammi, "A high-performance complexity reduced behavioral model and digital predistorter for MIMO systems with crosstalk," *IEEE Trans. Commun.*, vol. 64, no. 5, pp. 1996–2004, May 2016.
[20] K. G. Gard, H. M. Gutierrez, and M. B. Steer, "Characterization of spectral regrowth in microwave amplifiers based on the nonlinear transformation of a complex Gaussian process," *IEEE Trans. Microw. Theory Techn.*, vol. 47, no. 7, pp. 1059–1069, Jul. 1999.
[21] S. Blandino, C. Desset, A. Bourdoux, L. Van der Perre, and S. Pollin, "Analysis of out-of-band interference from saturated power amplifiers in massive MIMO," in *Proc. Eur. Conf. Netw. Commun. (EuCNC)*, Oulu, Finland, 2017, pp. 1–6.
[22] M. Alizadeh, S. Amin, and D. Rönnow, "Measurement and analysis of frequency-domain Volterra kernels of nonlinear dynamic 3 × 3 MIMO systems," *IEEE Trans. Instrum. Meas.*, vol. 66, no. 7, pp. 1893–1905, Jul. 2017.
[23] A. Mohammadi and F. M. Ghannouchi, *RF Transceiver Design for MIMO Wireless Communications*. Heidelberg, Germany: Springer, 2012.
[24] S. Wei, D. L. Goeckel, and P. A. Kelly, "Convergence of the complex envelope of bandlimited OFDM signals," *IEEE Trans. Inf. Theory*, vol. 56, no. 10, pp. 4893–4904, Oct. 2010.
[25] D. M. Pozar, *Microwave Engineering*, 4th ed. Hoboken, NJ, USA: Wiley, 2012.
[26] J. J. Bussgang, "Crosscorrelation functions of amplitude-distorted Gaussian signals," Res. Lab. Electron., Massachusetts Inst. Technol., Cambridge, MA, USA,Tech. Rep. 216, Mar. 1952.
[27] M. Isaksson, D. Wisell, and D. Rönnow, "A comparative analysis of behavioral models for RF power amplifiers," *IEEE Trans. Microw. Theory Techn.*, vol. 54, no. 1, pp. 348–359, Jan. 2006.
[28] I. Reed, "On a moment theorem for complex Gaussian processes," *IRE Trans. Inf. Theory*, vol. 8, no. 3, pp. 194–195, Apr. 1962.
[29] A. Zhu, P. J. Draxler, J. J. Yan, T. J. Brazil, D. F. Kimball, and P. M. Asbeck, "Open-loop digital predistorter for RF power amplifiers using dynamic deviation reduction-based Volterra series," *IEEE Trans. Microw. Theory Techn.*, vol. 56, no. 7, pp. 1524–1534, Jul. 2008.
[30] E. Björnson, P. Zetterberg, M. Bengtsson, and B. Ottersten, "Capacity limits and multiplexing gains of MIMO channels with transceiver impairments," *IEEE Commun. Lett.*, vol. 17, no. 1, pp. 91–94, Jan. 2013.
[31] P. Handel, "Power amplifier input back-off optimization in ideally predistorted OFDM systems," in *Proc. 3rd IEEE Int. Conf. Recent Trends Electron., Inf. Commun. Technol. (RTEICT)*, Bengaluru, India, May 2018, pp. 8–11.
[32] R. M. Corless, G. H. Gonnet, D. E. G. Hare, D. J. Jeffrey, and D. E. Knuth, "On the Lambert W function," *Adv. Comput. Math.*, vol. 5, no. 1, pp. 329–359, 1996.
[33] D. Tse and P. Viswanath, *Fundamentals of Wireless Communication*. Cambridge, U.K.: Cambridge Univ. Press, 2005.
[34] J. Chani-Cahuana, "Digital compensation techniques for power amplifiers in radio transmitters," Ph.D. dissertation, Dept. Elect. Eng., Chalmers Univ. Technol., Göthenburg, Sweden, 2017.
[35] H. Ochiai and H. Imai, "Performance of the deliberate clipping with adaptive symbol selection for strictly band-limited OFDM systems," *IEEE J. Sel. Areas Commun.*, vol. 18, no. 11, pp. 2270–2277, Nov. 2000.

Peter Händel (S'88–M'94–SM'98) received the M.Sc. degree in engineering physics and the Lic.Eng. and Ph.D. degrees in automatic control from the Department of Technology, Uppsala University, Uppsala, Sweden, in 1987, 1991, and 1993, respectively. He held a part-time position as an Associate Director of research with the Swedish Defense Research Agency from 2000 to 2006. In 2010, he joined the Indian Institute of Science, Bangalore, India, as a Guest Professor. He was a Guest Professor with the University of Gävle between 2007 and 2013. Since 1997, he has been with the Royal Institute of Technology (KTH), Stockholm, Sweden, where he is currently a Professor of signal processing with the School of Electrical Engineering and Computer Science. He has authored over 300 scientific publications. He was a recipient of a number of awards, including the IEEE Transactions on ITS Best Survey Paper Award. He is the former President of the IEEE Finland Joint Signal Processing and Circuits and Systems Chapter and the former President of the IEEE Sweden Signal Processing Chapter. He was an Associate Editor of the IEEE TRANSACTIONS ON SIGNAL PROCESSING.

Daniel Rönnow (M'04) received the M.Sc. degree in engineering physics and the Ph.D. degree in solid-state physics from Uppsala University, Uppsala, Sweden, in 1991 and 1996, respectively. He was with the Max-Planck-Institut für Festkörperforschung, Stuttgart, Germany, from 1996 to 1998, where he focused on semiconductor physics. He was with Acreo AB, Stockholm, Sweden, from 1998 to 2000, where he focused on infrared sensors and systems. From 2000 to 2004, he was a Technical Consultant and the Head of Research with Racomna AB, Uppsala. From 2004 to 2006, he was a University Lecturer with the University of Gävle, Gävle, Sweden, where he became a Professor in electronics in 2011. From 2006 to 2011, he was a Senior Sensor Engineer with WesternGeco, Oslo, Norway, where he focused on signal processing and seismic sensors. He has been an Associate Professor with Uppsala University since 2000. He has authored or co-authored over 60 peer-reviewed papers and holds eight patents. His current research interests are RF measurement techniques and linearization of nonlinear RF circuits and systems.